Predicting Gemcitabine Delivery by ^{18}F-FAC PET in Murine Models of Pancreatic Cancer

James Russell[1], Milan Grkovski[1], Isabella J. O'Donoghue[1], Teja M. Kalidindi[2], Nagavarakishore Pillarsetty[2], Eva M. Burnazi[3], Amanda Kulick[4], Amber Bahr[4], Qing Chang[4], H. Carl LeKaye[1], Elisa de Stanchina[4], Kenneth H. Yu[5], and John L. Humm[1]

[1]Department of Medical Physics, Memorial Sloan Kettering Cancer Center, New York, New York; [2]Department of Radiology, Memorial Sloan Kettering Cancer Center, New York, New York; [3]Radiochemistry and Molecular Imaging Probe Core Facility, Memorial Sloan Kettering Cancer Center, New York, New York; [4]Anti-Tumor Assessment Core Facility, Memorial Sloan Kettering Cancer Center, New York, New York; and [5]Department of Medicine, Memorial Sloan Kettering Cancer Center, New York, New York

^{18}F-FAC (2′-deoxy-2′-^{18}F-fluoro-β-D-arabinofuranosylcytosine) has close structural similarity to gemcitabine and thus offers the potential to image drug delivery to tumors. We compared tumor ^{18}F-FAC PET images with ^{14}C-gemcitabine levels, established ex vivo, in 3 mouse models of pancreatic cancer. We further modified tumor gemcitabine levels with injectable PEGylated recombinant human hyaluronidase (PEGPH20) to test whether changes in gemcitabine would be tracked by ^{18}F-FAC. **Methods:** ^{18}F-FAC was synthesized as described previously. Three patient-derived xenograft (PDX) models were grown in the flanks of NSG mice. Mice were given PEGPH20 or vehicle intravenously 24 h before coinjection of ^{18}F-FAC and ^{14}C-gemcitabine. Animals were euthanized and imaged 1 h after tracer administration. Tumor and muscle uptake of both ^{18}F-FAC and ^{14}C-gemcitabine was obtained ex vivo. The efficacy of PEPGPH20 was validated through staining with hyaluronic acid binding protein. Additionally, an organoid culture, initiated from a KPC (Pdx-1 Cre LSL-Kras^{G12D} LSL-p53^{R172H}) tumor, was used to generate orthotopically growing tumors in C57BL/6J mice, and these tumors were then serially transplanted. Animals were injected with PEGPH20 and ^{14}C-gemcitabine as described above to validate increased drug uptake by ex vivo assay. PET/MR images were obtained using a PET insert on a 7-T MR scanner. Animals were imaged immediately before injection with PEGPH20 and again 24 h later. **Results:** Tumor-to-muscle ratios of ^{14}C-gemcitabine and ^{18}F-FAC correlated well across all PDX models and treatments (R^2 = 0.78). There was a significant increase in the tumor PET signal in PEGPH20-treated PDX animals, and this signal was matched in ex vivo counts for 2 of 3 models. In KPC-derived tumors, PEGPH20 raised ^{14}C-gemcitabine levels (tumor-to-muscle ratio of 1.9 vs. 2.4, control vs. treated, P = 0.013). PET/MR ^{18}F-FAC images showed a 12% increase in tumor ^{18}F-FAC uptake after PEGPH20 treatment (P = 0.023). PEGPH20-treated animals uniformly displayed clear reductions in hyaluronic acid staining. **Conclusion:** ^{18}F-FAC PET was shown to be a good surrogate for gemcitabine uptake and, when combined with MR, to successfully determine drug uptake in tumors growing in the pancreas. PEGPH20 had moderate effects on tumor uptake of gemcitabine.

Received Apr. 8, 2020; revision accepted Jun. 15, 2020.
For correspondence or reprints contact: John L. Humm, Department of Medical Physics, Memorial Sloan Kettering Cancer Center, 1275 York Ave., New York, NY 10065.
E-mail: hummj@mkscc.org
Published online Jul. 9, 2020.

Key Words: ^{18}F-FAC; gemcitabine; drug delivery; hyaluronic acid; pancreatic cancer; PET/MRI

J Nucl Med 2021; 62:195–200
DOI: 10.2967/jnumed.120.246926

Pancreatic ductal adenocarcinoma (PDAC) is the most lethal common solid malignancy, with an increasing incidence and a dismal 5-y relative survival rate of 9% (*1*). Although the reasons for this lethality are multifactorial (*2*), inefficient drug delivery due to the dense desmoplastic stroma that surrounds malignant epithelial cells—a unique morphologic feature of pancreatic cancer that results in elevated interstitial pressure (*3*)—is believed to be among the main contributors to chemoresistance (*4*). A significant increase in the survival of PDAC patients was observed with the introduction of combination therapy regimens (*5–7*), suggesting unmet opportunities in drug development.

There is an urgent need to develop and use noninvasive biomarkers for, first, quantification of intratumor drug uptake before or during therapy; second identification of patients who may potentially benefit from interventions designed to improve tumor drug penetrance; and, third, determination of the optimal time-window during which the stromal burden remains reduced. Providing a capability to measure drug uptake noninvasively using a surrogate PET radiotracer would allow changes in drug uptake to be determined as a consequence of treatment intervention. It is currently unknown whether a specific treatment, such as radiation therapy, increases or decreases chemotherapeutic drug uptake, as there are no available methods to measure these changes.

Gemcitabine is a chemotherapy drug that has been widely used to treat patients with surgically resectable and advanced PDAC. Deoxycytidine kinase is a rate-limiting enzyme in deoxyribonucleoside salvage, a metabolic pathway involved in the production and maintenance of a balanced pool of deoxyribonucleoside triphosphates for DNA synthesis. Imaging probes that target deoxycytidine kinase may allow for patient stratification into likely responders and nonresponders with deoxycytidine kinase–dependent prodrugs such as gemcitabine (*8,9*). ^{18}F-FAC (2′-deoxy-2′-^{18}F-fluoro-β-D-arabinofuranosylcytosine) is a PET imaging agent first developed by Radu's group (*10,11*). It is a substrate for deoxycytidine kinase with an affinity similar to that of gemcitabine. Whereas gemcitabine has a

double substitution of a hydrogen atom with a fluorine compared with deoxycytidine, ^{18}F-FAC has a single substitution. ^{18}F-FAC PET dosimetry studies demonstrated that the probe can safely be used to image the deoxyribonucleoside salvage pathway in humans (*9*).

We have developed a clinically translatable methodology for the synthesis of ^{18}F-FAC (*12*) and demonstrated that ^{18}F-FAC uptake reflects gemcitabine distribution in human orthotopic and genetically modified murine pancreatic cancer models (*13*). The principal aim of this study was to validate whether ^{18}F-FAC PET reflects gemcitabine levels in different patient-derived xenograft (PDX) models of pancreatic cancer. We also investigated whether the intratumor uptake of ^{18}F-FAC would increase in response to treatment with the stromal modulating agent PEGylated recombinant human hyaluronidase (PEGPH20). PEGPH20 degrades hyaluronic acid, a major component of the pancreatic cancer stroma (*14,15*). It has been shown to be effective in enhancing drug uptake in preclinical models of pancreatic cancer (*16*). Although it has recently failed to improve therapeutic outcomes (*17*), it can serve as a means to manipulate stroma in experimental tumors.

MATERIALS AND METHODS

Animals and Tumor Models

All procedures involving animals were approved by the Institutional Animal Care and Use Committee of Memorial Sloan Kettering Cancer Center. Similarly, the animals used in this study were cared for in accordance with guidelines approved by the Institutional Animal Care and Use Committee and Research Animal Resource Center.

Orthotopic murine tumors were established and serially transplanted in female C57BL/6 mice (Jackson Laboratory). The source material was derived from an organoid culture of cells taken from a genetically engineered mouse (Pdx1-Cre;LSL-KRASG12D;Trp53R172H/wt). The culture was a generous gift of Dr. David A. Tuveson, Cold Spring Harbor, NY. Tumor fragments (~2 mm) were transplanted as follows. The mice were anesthetized by isoflurane inhalation (2%; flow rate, 1 L/min) and administered a 2 mg/kg dose of meloxicam and a 0.5 mg/kg dose of buprenorphine subcutaneously as preemptive analgesia. The area of the left abdominal wall was shaved, and sterilizing scrubs were applied before a 1-cm incision was made. The spleen and pancreas were exteriorized, and the tumor graft was fixed to the pancreas with ligature (4-0 Vicryl, polyglactin 910; Ethicon). The muscle layer was closed using Vicryl, the skin edges were closed with sterilized wound clips, and a local anesthetic (bupivacaine) was applied at the incision edges. Postoperative care included close monitoring of the animals and administration of meloxicam once per day for 2 d as analgesia. Wound clips were removed 1 wk after surgery.

NOD.Cg-Prkdcscid Il2rgtm1Wjl/SzJ (NSG) mice (Jackson Laboratory) were used for PDX generation as follows: 6-wk-old female NSG mice were implanted subcutaneously with specimens freshly collected from patients at Memorial Sloan Kettering Cancer Center under an approved institutional review board biospecimen protocol, as previously described (*18*). Tumors developed 2–4 mo after implantation. They were expanded into further mice by serial transplantation. The generated PDXs were subjected to high-coverage next-generation sequencing with the Memorial Sloan Kettering IMPACT (integrated mutation profiling of actionable cancer targets) assay.

Radiotracers

^{18}F-FAC was synthesized using a method slightly modified from that reported in our previous publication (*12,19*). Briefly, ^{18}F in the form of [^{18}F]HF was loaded onto a quaternary methyl ammonium cartridge preconditioned by passing 5 mL of 0.25 M $KHCO_3$ followed by 20 mL of deionized water and eluted with 1 mL of 90% acetonitrile in water solution, containing $KHCO_3$ (1.6 mg, 15.9 μmol) and Kryptofix (Merck) (10 mg, 26.4 μmol), into a 10-mL Reacti-Vial (Pierce Chemical). The solution was evaporated by heating the vial to 110°C under a slow stream of argon gas. To the dried vial, an additional 0.5 mL of anhydrous acetonitrile was added, and the solvent was removed as described above and the whole process was repeated 2 additional times. To the vial, 15 mg of the triflate precursor (2-*O*-(trifluoromethylsulfonyl)-1,3,5-tri-*O*-benzoyl-α-D-arabinofuranose) dissolved in 400 μL of acetonitrile were added and the reaction mixture was heated at 110°C for 30 min. The reaction mixture was cooled and transferred to a microwave vial containing cytosine silyl ether (*N*-(trimethylsilyl)-2-((trimethylsilyl)oxy)pyrimidin-4-amine, 25 mg) in a 500-μL solution of acetonitrile, trimethylsilyltriflate, and hexamethyldisilane (3:1:1) and heated using a microwave oven at 120°C for 25 min. The reaction mixture was cooled to room temperature and passed through a silica Sep-Pak Plus column (Waters) (preconditioned with 5 mL of hexane) and eluted into a 10-mL Reacti-Vial with 10% MeOH in CH_2Cl_2 (2 × 1.25 mL). The solvents were removed by heating the Reacti-Vial under an argon flow at 110°C. To the crude reaction mixture, 0.3 mL of 4.6 M sodium methoxide in MeOH (25% w/v) was added and the reaction mixture was heated at 80°C for 10 min for deprotection. The reaction mixture was treated with glacial acetic acid (120 μL), and the solvent was removed under an argon stream at 80°C. The residue was dissolved in 1.8 mL of water passed through a C18-mini column (Strata C18-E [55 μm, 70 Å], 50 mg/1 mL) to remove insoluble impurities. The crude product was purified using reversed-phased high-performance liquid chromatography (C18, XBridge 5 μm, 10 × 250 mm [catalog no. 186008167; Waters]) with an isocratic solvent system of 1% acetonitrile in 0.1% trifluoroacetic acid in water. The radioactive fraction corresponding to the product peak ^{18}F-FAC was collected, and solvent was evaporated under reduced pressure. The identity of the product ^{18}F-FAC was verified by coinjecting with a commercially available nonradioactive analog on a high-performance liquid chromatography analytic column (Gemini 5 μm, 250 × 4.6 mm, 110 Å [catalog no. 00G-4435-E0; Phenomenex]) with an isocratic solvent system of 2% acetonitrile in 0.1% trifluoroacetic acid in water.

PET Imaging

Orthotopically implanted animals were treated approximately 2–3 wk after implantation. At this stage, tumors were already approximately 10–15 mm in diameter. PDX tumors were markedly ellipsoid in shape, and the animals were treated when the long diameter was approximately 10 mm. The animals received either vehicle (saline) or PEGPH20 (10 μg/animal; Halozyme) via the tail vein. Twenty-four hours later, the animals were injected intraperitoneally with approximately 11 MBq of ^{18}F-FAC, approximately 0.037 MBq of ^{14}C-gemcitabine (Moravek Biochemicals), or both. The ^{18}F activity in each syringe was measured, along with the times of measurement and injection, and was used to establish the exact injected ^{14}C activity. PET images of PDX tumors were a single acquisition comparing control and PEGPH20-treated animals. The animals were euthanized with CO_2 inhalation 1 h after tracer injection, and the carcasses were imaged on a Focus 120 microPET (Siemens), in a 5-min acquisition. The photon energy window was 350–750 keV, and the coincidence timing window was 6 ns. Fourier rebinning was used to sort data into 2-dimensional histograms, and transverse images were reconstructed using an ordered-subset expectation maximization algorithm into a 128 × 128 × 63 (0.72 × 0.72 × 1.3 mm) matrix. The image data were normalized to correct for dead-time count losses, nonuniformity of response of the PET, positron branching ratio, and radioactive decay before injection. No attenuation, scatter, or partial-volume averaging correction was applied. An empirically determined system calibration factor for mice was used to convert voxel count rates to activity concentrations.

The resulting image data were then normalized to the administered activity to parameterize images in terms of percentage injected dose (%ID)/g.

PET/MRI

A 7-T MR–compatible PET insert was custom-designed and built for the 7-T Biospec scanner (Bruker Biospin Corp.) with a 20-cm bore and a maximum 100 mT/m field strength gradient. The scanner uses the more stable silicon photomultipliers as PET detectors (*20*). The PET insert has an axial field of view of 55 mm and a transaxial coverage of about 60 mm and is able to achieve a spatial resolution of less than 1.25 mm in reconstructed images.

The mice were injected with approximately 11 MBq of ^{18}F-FAC via the tail vein and were allowed free activity in the cage before the PET/MR scan. The mice were anesthetized by 2% isoflurane in oxygen and placed prone in the PET/MR scanner, with their respiration monitored by a physiologic monitoring system (SA Instruments). PET data were acquired in list mode 40 min after the injection for 20 min. Simultaneous 3-dimensional MRI of the mouse body was performed using a 300-MHz mouse volume coil (Doty Scientific). Mouse-body fast spin-echo RARE (rapid acquisition with relaxation enhancement) T2-weighted 3-dimensional MRI has a field of view of 6 × 3.5 × 3 cm and a voxel size of 0.23 × 0.27 × 0.31 mm, repetition time of 0.8 s, echo time of 47 ms, and RARE factor of 16.

PET images were processed off-line on a Linux workstation running a custom-written 3-dimensional ordered-subset expectation maximization reconstruction method (4 iterations and 16 subsets) resulting in an image matrix of 96 × 96 × 96 (0.6-mm voxels). Data were processed without correction for attenuation or scatter. Corrections for random coincidences and dead time were enabled. The image alignment was previously confirmed with a PET/MRI phantom. The resulting rigid-body transformation was then applied to the acquired animal PET datasets. Tumor ^{18}F-FAC intensity was quantified from tumor volume of interest defined in the coregistered MR images. Absolute trace uptake is expressed as %ID/g. Appropriate decay correction was applied to the time of injection.

Ex Vivo Counting

Carcasses were dissected and tumor and muscle removed. Tumor was divided for cryosectioning and ex vivo counting. ^{18}F activity was counted on a Wizard 1480 automatic γ-counter (Perkin Elmer) ^{14}C was counted on a Tri Carb 2910 TK scintillation counter (Perkin Elmer). ^{18}F counts were obtained immediately after dissection; tissue was then weighed and solubilized for ^{14}C scintillation counting. Solubilization was performed in Solvable (Perkin Elmer; 500 μL Solvable/150 mg of tissue, incubated for 1 h at 60°C, followed by 100 μL of hydrogen peroxide). Samples were counted in Ultima Gold (Perkin Elmer). An aliquot of the injection mix was retained and counted to allow ^{14}C results to be expressed in terms of the injected dose.

Hyaluronic Acid Staining

To validate the effect of PEGPH20 injection on tumor hyaluronic acid levels, cryosections were cut and stained with biotinylated hyaluronic acid binding protein (Millipore). Tumor was frozen in optimal-cutting-temperature compound (Sakura Finetek), and 10-μm sections were cut. Sections were fixed in 4% paraformaldehyde in phosphate-buffered saline for 10 min and washed twice in phosphate-buffered saline. Endogenous peroxidase was quenched by 15-min exposure to sodium azide (0.5%) and hydrogen peroxide (0.3%) in ultrapure water, followed by application of an avidin biotin blocking kit (Vector Labs) according to the manufacturer's instructions. Sections were blocked with 1% bovine serum albumin for 1 h at room temperature, followed by hyaluronic acid binding protein (5 μg/mL) overnight at 4°C. Sections were washed 3 times in phosphate-buffered saline and labeled with horseradish peroxidase using the ABC kit (Vector Labs); color was developed with diamino benzidine/hydrogen peroxide (Vector Labs), all according to the manufacturer's instructions. Sections were counterstained with Hematoxylin Quick Stain (Vector Labs).

Statistics

Coefficients of determination (R^2) measuring the association between ^{18}F-FAC and ^{14}C-gemcitabine were obtained from linear regression performed in Excel; the null hypothesis that ^{14}C-gemcitabine and ^{18}F-FAC uptake was not greater after PEGPH20 treatment was tested by the 1-tailed Mann–Whitney test, except in the case of mice imaged before and after treatment, for which a 1-tailed paired *t* test (Excel) was applied. All *P* values are presented in the text.

RESULTS

The PDX strains used in this study were LoweM_PAAD1a, RomeP_PAAD_x0002a, and RomeP_PAAD_x0005aS. For simplicity, we refer to them as 1a, X0002, and X0005. Mice bearing PDX tumors were coinjected with ^{14}C-gemcitabine and ^{18}F-FAC. There were 10 mice per PDX model, of which 5 were given vehicle and 5 PEGPH20. To validate ^{18}F-FAC as a surrogate for gemcitabine, ^{18}F activity was compared with ^{14}C-gemcitabine. Data derived from ex vivo counting correlated well (R^2 = 0.78, pooled data from 30 mice; Fig. 1A). Correlation was also high when tumor activity derived from the ^{18}F-FAC PET images was compared with ex vivo ^{14}C-gemcitabine tumor activity (R^2 = 0.79, Fig. 1B). The ^{18}F dynamic range of tumor-to-muscle ratios (Fig. 1A) was lower than that for the results expressed in %ID/g (Fig. 1B). This difference may be due to muscle uptake, as PEGPH20-treated mice displayed increased tumor and muscle levels of ^{18}F-FAC and ^{14}C-gemcitabine.

PEGPH20 was successful in reducing tumor hyaluronic acid (Fig. 2) in these animal models. There was notably less staining in tumors from PEGPH20-treated mice, uniformly observed in all experiments. In line with expectations, treatment with PEGPH20 increased the absolute ex vivo ^{14}C-gemcitabine tumor uptake in the X0002 and X0005 models (P = 0.008 and 0.033, respectively), though in the 1a model, significance was not reached (P = 0.37) (Fig. 2C). Similarly, tumor uptake of ^{18}F-FAC was increased in PEGPH20-treated mice (Fig. 2D). P values were 0.016 for 1a and X0002a and 0.0083 for X0005. This effect was observed when results were presented

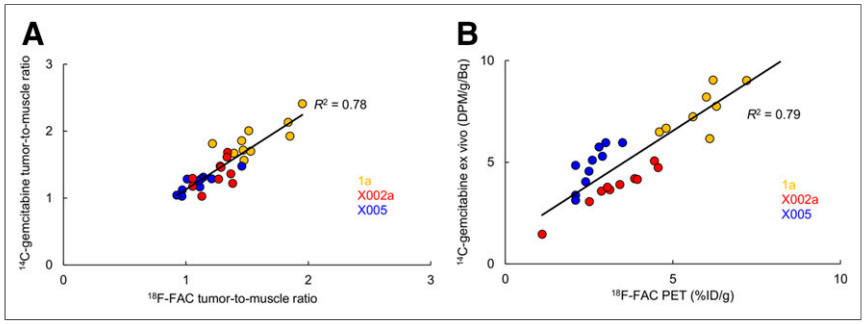

FIGURE 1. Correlation between ^{18}F-FAC and ^{14}C-gemcitabine, measured by ex vivo counting of both isotopes (A) and comparing activity in ^{18}F-FAC PET images with ^{14}C activity in tumor ex vivo (B). DPM = disintegrations per minute.

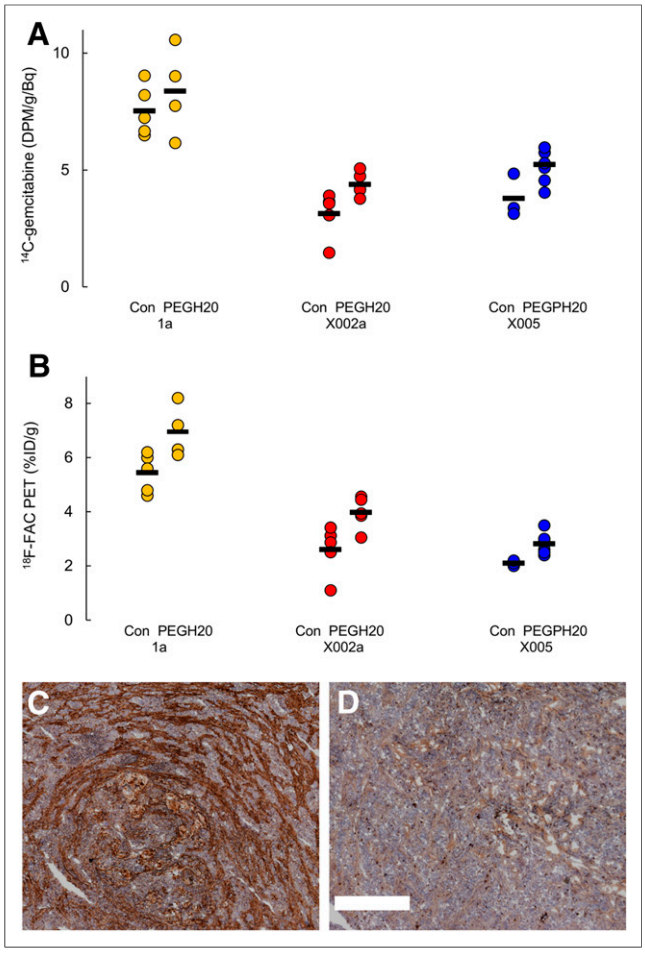

FIGURE 2. (A and B) Effect of PEGPH20 on ^{14}C-gemcitabine, measured ex vivo (A), and ^{18}F-FAC, quantified by PET (B). Mean value for each group is indicated by black line. Significance ($P < 0.05$) between control and PEGPH20 was observed for all cases except ^{14}C-gemcitabine in PDX 1a. Data are from same experiment as in Figure 1. (C and D) Hyaluronidase staining (brown) in representative sections of control PDX 1a tumor (C) and PEGPH20-treated tumor (D). Scale bar = 500 μm.

in terms of tumor activity–to–injected activity ratio. However, a significant effect of PEGPH20 on tracer and gemcitabine uptake was not seen when the results were presented as tumor-to-muscle ratios (Supplemental Fig. 1; supplemental materials are available at http://jnm.snmjournals.org), and in fact PEGPH20 consistently raised muscle ^{18}F-FAC counts in these experiments, by about 30%.

PEGPH20 pretreatment resulted in increased levels of ^{14}C-gemcitabine uptake in KPC (Pdx-1 Cre LSL-Kras^{G12D} LSL-p53^{R172H})–derived tumors growing orthotopically in the pancreas (Fig. 3). In terms of disintegrations/min per gram, there was approximately 60% more activity in tumors from PEGPH20-treated mice ($P = 0.016$). For this model, the tumor-to-muscle ratios of ^{14}C-gemcitabine were also significantly elevated (29%, $P = 0.004$; Supplemental Fig. 1), and biodistributions of ^{14}C-gemcitabine in C57BL/6 mice were not altered by PEGPH20 treatment (Supplemental Figs. 2 and 3). Thus, it seems that the different strains of mice respond differently to PEGPH20. There is no mechanistic explanation that we know of to account for these observations; however, as we were interested primarily in the ability of ^{18}F-FAC to serve as a surrogate for gemcitabine, we chose not to further investigate the normal-tissue response to PEGPH20.

Six animals with KPC-derived orthotopic tumors were imaged with ^{18}F-FAC PET/MR before and 24 h after administration of PEGPH20 (Fig. 4). Whole-tumor uptake of ^{18}F-FAC increased on average by 12%, rising from 1.59 ± 0.24 to 1.78 ± 0.29 % ID/g ($P = 0.012$, Fig. 5). The PET/MR images generally showed that ^{18}F-FAC activity was peripheral in these tumors, both before and after PEGPH20 treatment. Qualitatively, this was similar to what was observed in ^{18}F-FAC autoradiographs obtained in a separate experiment (Supplemental Fig. 4).

DISCUSSION

A methodology to noninvasively quantify drug uptake in tumors would be of immense value, allowing strategies purporting to enhance drug uptake to be assessed on a patient-by-patient basis. Our study showed that ^{18}F-FAC correlated strongly with tumor gemcitabine levels in PDX models of pancreatic disease. We demonstrated that an intervention (PEGPH20) that would increase intratumor accumulation of gemcitabine would also lead to increased intratumor ^{18}F-FAC. Experiments with the PDX models supplied direct evidence for this hypothesis, as we achieved ^{18}F-FAC and ^{14}C-gemcitabine quantification in the same mice. For the orthotopic tumors, by contrast, evidence was indirect—a treatment that increased tumor gemcitabine levels in one cohort of mice increased intratumor accumulation of ^{18}F-FAC in a different group of animals. ^{18}F-FAC quantification was by PET/MR, as ^{18}F-FAC PET imaging of such tumors could not be accomplished without independent tumor delineation. With this in place, PET/MR images of ^{18}F-FAC in tumors before and after PEGPH20 injection yielded evidence of an enhancement of ^{18}F-FAC after PEGPH20 treatment consistent with the ^{14}C-gemcitabine drug uptake values. The successful imaging and quantitation of ^{18}F-FAC in tumors growing in the pancreas support the belief that this technology can be transferred to the clinic.

As regards PEGPH20, from preclinical studies it had seemed a promising way to increase drug access to pancreatic tumors. However, it recently failed a phase III clinical trial (HALO-301 (*17*)) and was withdrawn from development. Although PEGPH20 clearly affected gemcitabine uptake in our models, there were some inconsistencies in the data. For the PDX tumors in NSG mice, PEGPH20 led to a clear increase in tumor gemcitabine, though as there also was increased ^{18}F-FAC in normal tissues, this gemcitabine increase was not reflected in the tumor-to-muscle ratio. By contrast, in the C57BL/6 mice, biodistribution studies of ^{14}C gemcitabine suggested that PEGPH20 affected drug uptake only in tumor tissue. In these animals, PEGPH20 treatment resulted in a significant increase in the tumor-to-muscle ratio of ^{14}C-gemcitabine. It may be that the 2 strains of mice respond differently to PEGPH20, but we did not choose to investigate this possibility, particularly in view of the failure to enhance clinical outcomes through PEGPH20 administration.

PEGPH20 was the second major attempt to improve drug access to pancreatic cancer, after the initial failure of hedgehog pathway inhibitors (*21,22*). Other attempts to increase drug delivery in pancreatic cancer are ongoing (*23–26*), and if any such strategy is to be transferred to the clinic, a direct assessment of tumor gemcitabine could be invaluable. Judging such a strategy simply by patient survival alone is problematic, since in the treatment group there will be

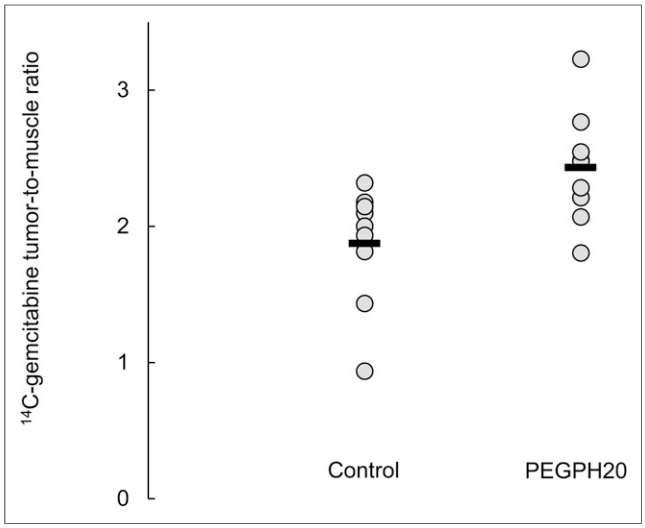

FIGURE 3. Effect of PEGPH20 on ^{14}C-gemcitabine uptake in KPC-derived tumors growing orthotopically in pancreas. Mean value for each group is indicated by black line. Significant difference ($P < 0.05$) was found.

individuals whose tumors are inherently resistant to gemcitabine (*27*) and, very likely, also interpatient variability in response to the antistromal agent. The results presented here establish ^{18}F-FAC PET as a potentially informative imaging modality in this context, since it both correlates well with gemcitabine delivery and can quantify changes in tumor gemcitabine brought about by antistromal treatment.

In addition to predicting the total tumor gemcitabine accumulation, ^{18}F-FAC PET also revealed significant tumor heterogeneity,

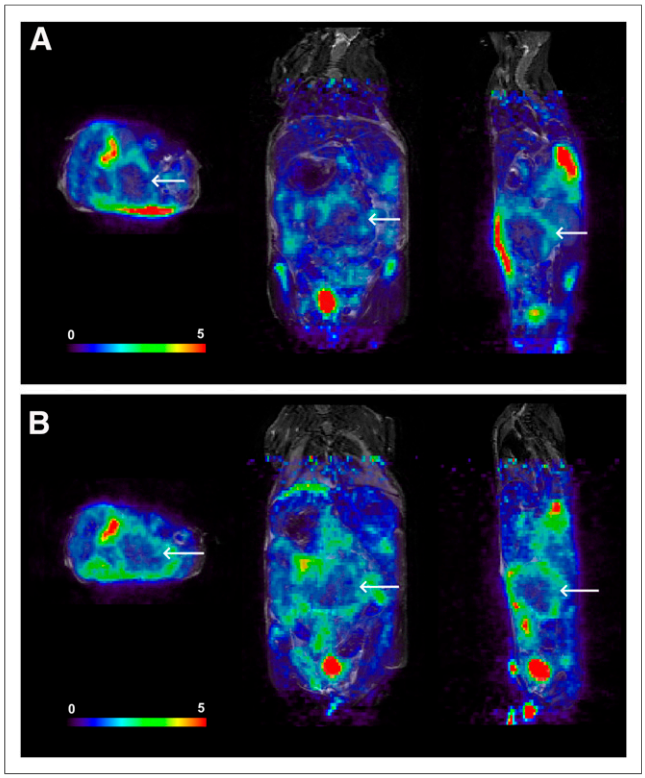

FIGURE 4. ^{18}F-FAC PET/MRI of mouse before (A) and 24 h after (B) injection of PEGPH20. Scale bar represents %ID/g. Tumor is indicated by arrows. Mean intratumor ^{18}F-FAC uptake increased from 1.42 to 1.76 %ID/g.

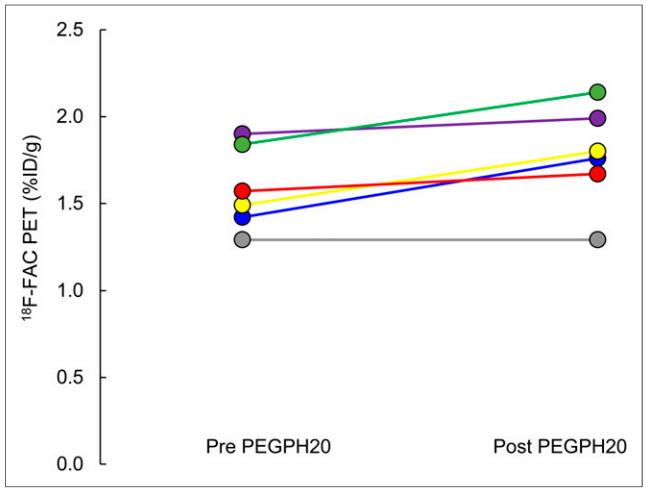

FIGURE 5. ^{18}F-FAC uptake as measured by PET/MRI increases after PEGPH20 injection in KPC-derived orthotopic tumors, from 1.59 ± 0.24 to 1.78 ± 0.29 %ID/g.

seen in PET images obtained from the PDX- and KPC-derived models, and present both in control and in PEGPH20-treated animals and mirrored by autoradiography. Heterogeneity of drug distribution in tumors will be a major barrier to successful therapy, as tumor response will be determined by the least-treated population. For any strategy based on increasing drug uptake, this consideration is a critical one that can be understood only through imaging. In pancreatic tumors, the stromal barriers that limit drug uptake also create uneven drug distribution (*28*). Heterogeneity in gemcitabine uptake could also arise from variable expression levels of deoxycytidine kinase, which largely determine its accumulation and efficacy (*29*). However, in the KPC-derived tumors we have also mapped 5-fluorouracil distribution and found that it correlates closely with that of gemcitabine (*30*), though 5-fluorouracil entrapment is governed by an entirely separate pathway.

Finally, tumor-associated macrophages have recently been shown to interfere with gemcitabine response through the release of deoxycytidine (*31*), reducing gemcitabine efficacy in a murine model. Significantly, deoxycytidine does not inhibit cellular uptake of gemcitabine but, rather, inhibits DNA incorporation. The implication for the clinical use of ^{18}F-FAC might be that whereas low signal would likely identify minimal gemcitabine responders, a high PET signal would not in itself be a reliable promise of therapeutic benefit.

CONCLUSION

We have demonstrated a good concordance between ^{18}F-FAC and gemcitabine in 3 PDX models of pancreatic cancer. There was a significant correlation between tumor ^{18}F-FAC and ^{14}C-gemcitabine when both tracers were counted in dissected tissue; this correlation held when ^{18}F activity concentrations were obtained from PET images. The effects of PEGPH20 pretreatment on gemcitabine uptake could be predicted by ^{18}F-FAC imaging. In mouse models of pancreatic disease, ^{18}F-FAC PET has the ability to predict tumor gemcitabine levels and may be useful to assess techniques that purport to enhance tumor drug delivery.

DISCLOSURE

James Russell, Milan Grkovski, Isabella O'Donoghue, Nagavarakishore Pillarsetty, Kenneth Yu, and John Humm were funded in part by NIH

grant R01 CA194321 (principal investigator, John L. Humm). Carl LeKaye was funded through NIH Center grant RC2 CA148971 (principal investigator, Jason A. Koutcher). Amanda Kulick, Amber Bahr, Qing Chang, and Elisa de Stanchina were funded in part through NIH grant U54 OD020355 (principal investigator, Scott W. Lowe). James Russell, Nagavarakishore Pillarsetty, Kenneth Yu, and John Humm are partly supported by IMRAS grant GC259290 (principal investigator, John L. Humm). Research at Memorial Sloan Kettering Cancer Center is supported by NIH/NCI Cancer Center support grant P30 CA008748 (principal investigator, Craig B. Thompson). No other potential conflict of interest relevant to this article was reported.

ACKNOWLEDGMENTS

The PEGPH20 used for this study was provided as a generous gift from Halozyme Inc., San Diego, CA.

KEY POINTS

QUESTION: Can drug delivery of gemcitabine in pancreatic cancer be quantified through noninvasive PET imaging with ^{18}F-FAC?

PERTINENT FINDINGS: A good concordance was seen between ^{18}F-FAC and ^{14}C-gemcitabine uptake in 3 PDX models of pancreatic cancer. The effects of PEGPH20 pretreatment on gemcitabine uptake could be predicted by ^{18}F-FAC imaging.

IMPLICATIONS FOR PATIENT CARE: ^{18}F-FAC PET may be useful to assess techniques that purport to enhance drug delivery in pancreatic cancer.

REFERENCES

1. Siegel RL, Miller KD, Jemal A. Cancer statistics, 2020. *CA Cancer J Clin.* 2020;70:7–30.
2. Hruban RH, Gaida MM, Thompson E, et al. Why is pancreatic cancer so deadly? The pathologist's view. *J Pathol.* 2019;248:131–141.
3. DuFort CC, DelGiorno KE, Carlson MA, et al. Interstitial pressure in pancreatic ductal adenocarcinoma is dominated by a gel-fluid phase. *Biophys J.* 2016;110:2106–2119.
4. Olive KP, Jacobetz MA, Davidson CJ, et al. Inhibition of hedgehog signaling enhances delivery of chemotherapy in a mouse model of pancreatic cancer. *Science.* 2009;324:1457–1461.
5. Neoptolemos JP, Palmer DH, Ghaneh P, et al. Comparison of adjuvant gemcitabine and capecitabine with gemcitabine monotherapy in patients with resected pancreatic cancer (ESPAC-4): a multicentre, open-label, randomised, phase 3 trial. *Lancet.* 2017;389:1011–1024.
6. Conroy T, Hammel P, Hebbar M, et al. FOLFIRINOX or gemcitabine as adjuvant therapy for pancreatic cancer. *N Engl J Med.* 2018;379:2395–2406.
7. Tiriac H, Belleau P, Engle DD, et al. Organoid profiling identifies common responders to chemotherapy in pancreatic cancer. *Cancer Discov.* 2018;8:1112–1129.
8. Shu CJ, Campbell DO, Lee JT, et al. Novel PET probes specific for deoxycytidine kinase. *J Nucl Med.* 2010;51:1092–1098.
9. Schwarzenberg J, Radu CG, Benz M, et al. Human biodistribution and radiation dosimetry of novel PET probes targeting the deoxyribonucleoside salvage pathway. *Eur J Nucl Med Mol Imaging.* 2011;38:711–721.
10. Laing RE, Walter MA, Campbell DO, et al. Noninvasive prediction of tumor responses to gemcitabine using positron emission tomography. *Proc Natl Acad Sci USA.* 2009;106:2847–2852.
11. Radu CG, Shu CJ, Nair-Gill E, et al. Molecular imaging of lymphoid organs and immune activation by positron emission tomography with a new [^{18}F]-labeled 2′-deoxycytidine analog. *Nat Med.* 2008;14:783–788.
12. Gangangari KK, Humm JL, Larson SM, Pillarsetty NVK. TMSOTf assisted synthesis of 2′-deoxy-2′-[^{18}F]fluoro-beta-D-arabinofuranosylcytosine ([^{18}F]FAC). *PLoS One.* 2018;13:e0196784.
13. Russell J, Pillarsetty N, Kramer RM, et al. In vitro and in vivo comparison of gemcitabine and the gemcitabine analog 1-(2′-deoxy-2′-fluoroarabinofuranosyl) cytosine (FAC) in human orthotopic and genetically modified mouse pancreatic cancer models. *Mol Imaging Biol.* 2017;19:885–892.
14. Provenzano PP, Hingorani SR. Hyaluronan, fluid pressure, and stromal resistance in pancreas cancer. *Br J Cancer.* 2013;108:1–8.
15. Whatcott CJ, Diep CH, Jiang P, et al. Desmoplasia in primary tumors and metastatic lesions of pancreatic cancer. *Clin Cancer Res.* 2015;21:3561–3568.
16. Jacobetz MA, Chan DS, Neesse A, et al. Hyaluronan impairs vascular function and drug delivery in a mouse model of pancreatic cancer. *Gut.* 2013;62:112–120.
17. Hakim N, Patel R, Devoe C, Saif MW. Why HALO 301 failed and implications for treatment of pancreatic cancer. *Pancreas (Fairfax).* 2019;3:e1–e4.
18. Mattar M, McCarthy CR, Kulick AR, Qeriqi B, Guzman S, de Stanchina E. Establishing and maintaining an extensive library of patient-derived xenograft models. *Front Oncol.* 2018;8:19.
19. Zhang H, Cantorias MV, Pillarsetty N, Burnazi EM, Cai S, Lewis JS. An improved strategy for the synthesis of [^{18}F]-labeled arabinofuranosyl nucleosides. *Nucl Med Biol.* 2012;39:1182–1188.
20. Catana C, Wu Y, Judenhofer MS, Qi J, Pichler BJ, Cherry SR. Simultaneous acquisition of multislice PET and MR images: initial results with a MR-compatible PET scanner. *J Nucl Med.* 2006;47:1968–1976.
21. Gu J, Saiyin H, Fu D, Li J. Stroma: a double-edged sword in pancreatic cancer—a lesson from targeting stroma in pancreatic cancer with hedgehog signaling inhibitors. *Pancreas.* 2018;47:382–389.
22. De Jesus-Acosta A, Sugar EA, O'Dwyer PJ, et al. Phase 2 study of vismodegib, a hedgehog inhibitor, combined with gemcitabine and nab-paclitaxel in patients with untreated metastatic pancreatic adenocarcinoma. *Br J Cancer.* 2020;122:498–505.
23. Eberle-Singh JA, Sagalovskiy I, Maurer HC, et al. Effective delivery of a microtubule polymerization inhibitor synergizes with standard regimens in models of pancreatic ductal adenocarcinoma. *Clin Cancer Res.* 2019;25:5548–5560.
24. Chen X, Jia F, Li Y, et al. Nitric oxide-induced stromal depletion for improved nanoparticle penetration in pancreatic cancer treatment. *Biomaterials.* 2020;246:119999.
25. Dosch AR, Dai X, Reyzer ML, et al. Combined Src/EGFR inhibition targets STAT3 signaling and induces stromal remodeling to improve survival in pancreatic cancer. *Mol Cancer Res.* 2020;18:623–631.
26. Han H, Hou Y, Chen X, et al. Metformin-induced stromal depletion to enhance the penetration of gemcitabine-loaded magnetic nanoparticles for pancreatic cancer targeted therapy. *J Am Chem Soc.* 2020;142:4944–4954.
27. Yu KH, Ricigliano M, McCarthy B, et al. Circulating tumor and invasive cell gene expression profile predicts treatment response and survival in pancreatic adenocarcinoma. *Cancers (Basel).* 2018;10:467.
28. Provenzano PP, Cuevas C, Chang AE, Goel VK, Von Hoff DD, Hingorani SR. Enzymatic targeting of the stroma ablates physical barriers to treatment of pancreatic ductal adenocarcinoma. *Cancer Cell.* 2012;21:418–429.
29. Kroep JR, Loves WJ, van der Wilt CL, et al. Pretreatment deoxycytidine kinase levels predict in vivo gemcitabine sensitivity. *Mol Cancer Ther.* 2002;1:371–376.
30. Fanchon LM, Russell J, Pillarsetty N, et al. Comparing the intra-tumoral distribution of gemcitabine, 5-fluorouracil, and capecitabine in a murine model of pancreatic ductal adenocarcinoma. *PLoS One.* 2020;15:e0231745.
31. Halbrook CJ, Pontious C, Kovalenko I, et al. Macrophage-released pyrimidines inhibit gemcitabine therapy in pancreatic cancer. *Cell Metab.* 2019;29:1390–1399.e6.